Received: 7 January 2020 | Revised: 26 February 2020 | Accepted: 2 March 2020

DOI: 10.1111/ijac.13504

International Journal of Applied Ceramic Technology

ORIGINAL ARTICLE

Morphological characterization and photocatalytic efficiency measurements of pure silica transparent open-cell sponges coated with TiO_2

Frank B. Löffler[1] | **Fabian J. Altermann**[1] | **Ethel C. Bucharsky**[1] | **Karl G. Schell**[1] | **Maria L. Vera**[2] | **Hernan Traid**[2] | **Anabela Dwojak**[2] | **Marta I. Litter**[3]

[1]Institute for Applied Materials – Ceramic Materials and Technologies, Karlsruhe Institute of Technology (KIT), Karlsruhe, Germany

[2]Instituto de Materiales de Misiones, CONICET, Universidad Nacional de Misiones, Facultad de Ciencias Exactas, Químicas y Naturales, Posadas, Argentina

[3]IIIA – Instituto de Investigación e Ingeniería Ambiental, CONICET, Universidad de San Martín, San Martín, Argentina

Correspondence
Ethel C. Bucharsky, Institute for Applied Materials – Ceramic Materials and Technologies, Karlsruhe Institute of Technology (KIT), Haid-und-Neu Straße 7, 76131 Karlsruhe, Germany.
Email: ethel.bucharsky@kit.edu

Marta I. Litter, IIIA – Instituto de Investigación e Ingeniería Ambiental, CONICET, Universidad de San Martín, San Martín, Argentina.
Email: marta.litter@gmail.com

Funding information
German Research Foundation (DFG); CONICET; Agencia Nacional de Promoción Científica y Tecnológica (ANPCyT), Grant/Award Number: PICT-2015-208 and PICT-2017-2133; BioCriticalMetals – ERAMIN; SPUK – Strategic Partnership Universidad Nacional de San Martin, Argentina; UNSAM; Karlsruher Institute for Technologies, (KIT); Innovation und International

Abstract

Transparent glass sponges are a new class of materials that can potentially be used for effective light distribution in photocatalytic applications. In this work, transparent glass sponges are prepared by the polymer replica technique and coated with TiO_2 to obtain a highly efficient photocatalytic material. Necessary conditions for obtaining transparent open-celled glass sponges are presented. The structure is characterized by employing light microscopy and scanning electron microscopy. In addition, μ-computer tomography (μ-CT) volume image analysis was performed that allows the calculation of geometrical parameters like pore size and specific surface area (SSA) of the structure, required for application of the new material. For photocatalytic application, the sponges have been coated with titanium dioxide (TiO_2) by immersion in a suspension of TiO_2 nanoparticles. The activity of the resulting coatings has been tested with the model reaction of transformation of Cr(VI) to Cr(III) in aqueous solutions in the presence of EDTA at pH 2. The reaction kinetics could be adjusted to a pseudo-first order reaction and the obtained rate constants have been employed to evaluate the photocatalytic activity. The activity of the sponges has been compared with that of samples of glass plates coated with TiO_2; it has been found that the sponges exhibited a higher catalytic activity than the glass plates. The photocatalytic activity increased with the porosity of the sponges, and the optimum sample was determined based on its photocatalytic performance and its mechanical stability. The results are promissory for application in photoreactors for transformation of pollutants in water and air decontamination.

KEYWORDS

glass, heterogeneous photocatalysis, hexavalent chromium, porosity, surface, TiO_2

1 | INTRODUCTION

Transparent silica sponges are a new class of materials that, if conveniently modified with TiO_2, are promissory to be used in photoreactors for removal of pollutants from water and air. Because of their optical properties and resistance to chemical attack, glass sponges are suitable to operate in a wide range of conditions. The basic requirement for a high photoactivity of the materials is the proper distribution of light within the whole structure. Furthermore, a large surface of the material is needed to get a good contact of the pollutant with the photocatalyst, assuring a fast mass transfer. Therefore, for photocatalytic applications, only open-celled materials are optimal since closed pores make only a surface (and small) contribution to the activity. However, open porous glass sponges are not commercially available.

Accordingly, the first attempts were made with glass fiber mats, which showed consistently good results.1-3 An overview describing different designs in terms of the performance of photobioreactors is given in a recent review article.4 However, 2D-structured materials have disadvantages because of small light transmission, effects of reflection and refraction, and low surface area.5 The use of transparent glass sponges could overcome these problems. For example, by the use of glass sponges in a photobioreactor, the biomass production capabilities of *Chlamydomonas reinhardtii* was improved by about 25%.6

Different methods are known for preparing cellular materials.7-11 The most conventional technique is the replica procedure, also known as the Schwartzwalder method.12,13 For the successful preparation of transparent open-celled structures, three main topics have to be considered: (a) the preparation of stabilized high-concentrated aqueous slurries based on nanoscale SiO_2 powders, (b) the temperature for burning out the resulting polymer, and (c) the subsequent sintering of the remaining SiO_2 framework to allow the formation of transparent cellular bodies. The successful stabilization of water-based suspensions with nanoscaled silica is shown in a previous work where the preparation of transparent glass sponges via replica method is presented.14 Based on this, transparent sponges in a wider range of pore sizes for their potential use in water treatment devices were developed.15

For use of the transparent cellular material, the knowledge of its geometrical properties is necessary. In this study, these parameters have been derived from calculations based on datasets of μ-computer tomography (μ-CT) imaging. Increased resolution has enabled a tomographic insight into such materials that allows to analyze the structure with respect to geometrically characteristic parameters.16 Its application to reticulated structures can therefore give the most extended view into its details. Additionally, scanning electron microscopy (SEM) and light microscopy (LM) were used for characterization of the resulting transparent sponge structures.

Photocatalysts can be used in different forms. In most applications, they have been used as powders dispersed in the water to be purified. However, in this form, an additional costly step to remove the powder from the water has to be applied. To overcome this drawback, several ways of immobilizing TiO_2 on surfaces have been adopted.17-21

Thus, this article is aimed at the comparison of the photocatalytic activity of nanoparticle-TiO_2 layers applied on glass sponges with a variation of pore size and consequent different specific surfaces necessary for greater catalytic activity. The relationship of the geometric parameters of the sponges such as pores per inch (ppi) and porosity and the TiO_2 amount on the sponges was investigated. The activity has been tested using hexavalent chromium, a very toxic and carcinogenic pollutant. EDTA was used as a synergetic compound.22

2 | EXPERIMENTAL PROCEDURE

2.1 | Preparation of the sponges and TiO_2 coating

Nanoscale amorphous SiO_2 particles (Aerosil OX50, Evonik Degussa GmbH, Essen, Germany, with SSA of 50 $m^2\ g^{-1}$) were dispersed in water at 35.7 vol% solid loading. The pH was adjusted to 10 by the addition of 1 mol/L tetramethylammonium hydroxide (TMAH, Alfa Aesar). The viscosities of the slurries were measured at constant shear rate ramp from 0.1 to 100 s^{-1} at 20°C using a viscometer (RheoStress RS 600, ThermoHaake GmbH) equipped with a rotating disk spindle set.

As templates for the replica process, polyurethane sponges having 30-80 ppi (FoamPartner Fritz Nauer AG) with 30 × 10 × 10 mm dimensions, were used. The ppi value and its nomenclature always refer to the polymer sponges and could be higher for the sintered sponges. The polymeric sponges were coated employing well-dispersed SiO_2 slurries and compressed while submerged in order to coat the struts of the sponges. The impregnated polymer support was then removed from the slurry, and the excess material was squeezed from the foam. The coated polymers were dried for 24 hours at 40°C and 80% humidity. For burning out the polymer, the coated preforms were placed in an alumina crucible and heated in a furnace (Carbolite Gero) under an air flow rate of approximately 150-200 L h^{-1}. To allow the gradual diffusion of developed gases, the heating regime was carefully selected. Therefore, the heating rates were in the range between 1 and 2.5°C min^{-1}. At 200°C, 500°C, and 800°C, the temperature was kept constant for 1 hour in order to ensure some degree of thermal homogenization and to avoid a high buildup of pressure within the struts. After this thermal treatment, the

geometrical density of the remaining structure was measured. Subsequently, the samples were sintered in air atmosphere inside a chamber furnace (Nabertherm GmbH) at 1300°C with heating rates of 10°C min^{-1} and a dwell time of 12 minutes. The different parameters such as density and porosity of green bodies (materials obtained after the pre-step before sintering) and sintered sponges are compiled in Table 1.

For the phase identification after different thermal treatments, X-ray diffraction (XRD) patterns were recorded using a diffractometer operating with Cu-K_α radiation at 40 kV and 40 mA (D8 Advance, Bruker). Macroscopic analysis was performed by image analysis using a digital light microscope (LM, Keyence) and scanning electron microscopy (SEM, Nova NanoSEM 450, FEI). In addition, volume image analysis was performed using μ-CT (Zeiss Xradia 520 Versa), equipped with a tungsten anode, which was operated at an acceleration voltage U_{acc} = 80 kV, a filament current of I = 85-90 μA, and a power of 7 W. The optical magnifications were 0.4× and 4×. The total measurement time was 4 hours.

A 5 w/v% TiO_2 (Degussa, Evonik, P25 Aeroxide) suspension was prepared, adjusting the pH to 2.5 with $HClO_4$ (69%-72%, Sintorgan, Argentina). The suspension was homogenized for 10 minutes under ultrasonication (Testlab TB02TA, Argentina). After several wettability tests, which evidenced the formation of bubbles on and inside the sintered sponges, the TiO_2 coatings were made by direct immersion of the sponge in the P25 suspension for 5 minutes, applying a local vacuum system to remove the bubbles trapped inside of the sponges using a pump (Watson Marlow 313S). Only one TiO_2 layer was applied in this instance.

The coated sponges were rinsed with water to eliminate nonadhered particles of P25. Then, the coated sponges were drained at room temperature, dried in an oven (SanJor SL30C, Argentina) at 50°C for 12 hours and then thermally treated at 500°C for 1 hour, with a heating rate of 10°C min^{-1} in the oven (SIMCIC). Also, blanks of P25 on glass slides (22 × 20 mm), obtained under similar conditions but with three layers to load 2.1 mg of P25 on each plate, were prepared. For all samples, a gravimetric determination of the amount of deposited TiO_2 was attempted using an analytical balance (Denver Instrument APX-200, Cole-Parmer). From edges and corners of the 30 and 40 ppi sponges, small fragments of SiO_2 were broken and detached, which avoided this determination. In addition, the 20 ppi sponges were too fragile to coat them without breaking, whereby they could not be employed.

2.2 | Photocatalytic experiments

A 0.4 mmol/L $K_2Cr_2O_7$ (Biopack) aqueous solution containing 1 mmol/L EDTA (Riedel de Haën AG, Seelze) (1.25 EDTA/Cr(VI) molar ratio) was used for the photocatalytic tests. The initial pH was adjusted to 2 with $HClO_4$ (69%-72%, Sintorgan). The photocatalyst samples were immersed into 20 mL of this solution contained in cylindrical reactors (4.5 cm diameter and 6.8 cm high) under magnetic stirring (Velp multistirrer 6). Six samples were irradiated simultaneously using a UV lamp (BLV MHL-404) with $\lambda > 250$ nm, maximum emission at 365 nm. Between the UV lamp and the reactor, a water filter and a glass filter were located, to avoid the incidence of IR radiation and of UV wavelengths lower than 300 nm, respectively. The mean UV irradiance incident on the surface of the solution (E_0) was 3520 μW cm^{-2}, measured at 365 nm with a homemade Arduino-based radiometer. Prior to irradiation, the solutions were kept under stirring in the dark for 30 minutes, to assure the adsorption equilibrium between the pollutant and the photocatalyst. No significant changes in Cr(VI) concentration were observed after this dark period. Samples (50 μL) were taken at 15, 30, 60, 120, and 180 minutes and diluted in 3 mL of water for analysis (conductivity ≤ 0.05 μS cm^{-1}). Changes in Cr(VI) concentration were spectrophotometrically monitored through the diphenylcarbazide method at 540 nm (ASTM D 1687-9223) using a UV-Vis spectrophotometer (Shimadzu, UV-2550). Blanks in the absence of the photocatalyst and with the TiO_2-coated glass plates were performed. An error of 5% was assumed for the photocatalytic experiments. The fitting of the experimental points was made with Origin 8.0 software, with reduced c^2 as the iteration-ending criterion.

To evaluate the photocatalytic activity after reuse of the TiO_2-coated sponges, photocatalytic tests were performed three times with the same sample during 180 minutes each, under the same test conditions. After each test, the coated sponges were rinsed with water, drained, and dried at room temperature, without further treatment.

TABLE 1 Relative density and porosity of green bodies and sintered sponges produced with polyurethane templates with 30, 40, 45, 60, and 80 ppi

	Relative density (%)		Porosity (%)	
Template (ppi)	Green body	Sintered body	Green body	Sintered body
30	3.9	8.5	96.1	91.5
40	3.5	7.7	96.5	92.3
45	4.8	10.8	95.2	89.2
60	4.9	11.3	95.1	88.7
80	5.6	15.6	94.4	84.4

3 | RESULTS AND DISCUSSION

3.1 | Characterization of the suspension

In the wet processing of ceramics, the particles must be first dispersed, preventing the formation of aggregates. In order to identify a suitable pH range for the electrostatic stabilization of the silica particles, zeta potential measurements were performed with 10 w/V% silica-based water suspensions, which are shown in Figure 1.

It is known that silanol groups dissociate and ionize with increasing pH values. Consequently, the absolute value of the measured zeta potential increases with increasing pH, with the optimum pH around 8.5. However, due to the formation of hydrogen bonds between neutral and negatively charged silanol groups, which leads to gelation, a large increase in suspension viscosity is observed. Therefore, the weak acid-neutral pH range seems to be inappropriate for stabilization. Employing SiO_2 nanoparticles and an appropriate mixing process, it is possible to obtain high-concentrated slurries with solid loadings up to 35.7 vol%. High solid loadings are necessary to create a dense and stable coating of silica on top of the surface of the polymer template. In addition, an adjusted viscosity is needed not only to coat the polymer properly, but also to get rid of the excess suspension that do not fill the cells. For the dip-coating process, it is necessary to reach adequate viscosities. Figure 2 shows the viscosity of three suspensions with various solid loadings in dependence

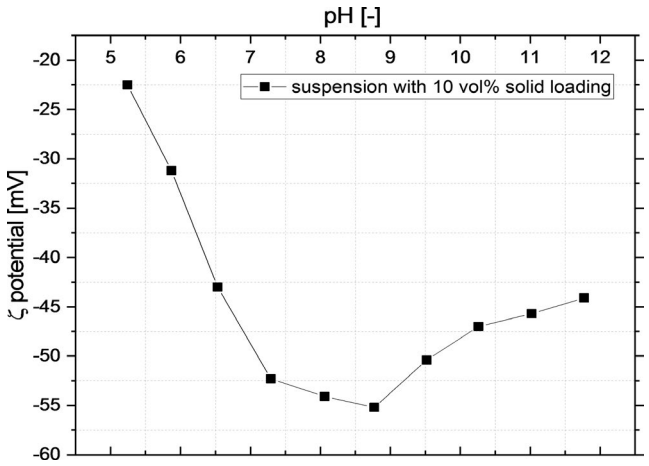

FIGURE 1 Variation of the zeta potential of 10 vol% silica–based water suspensions with pH value

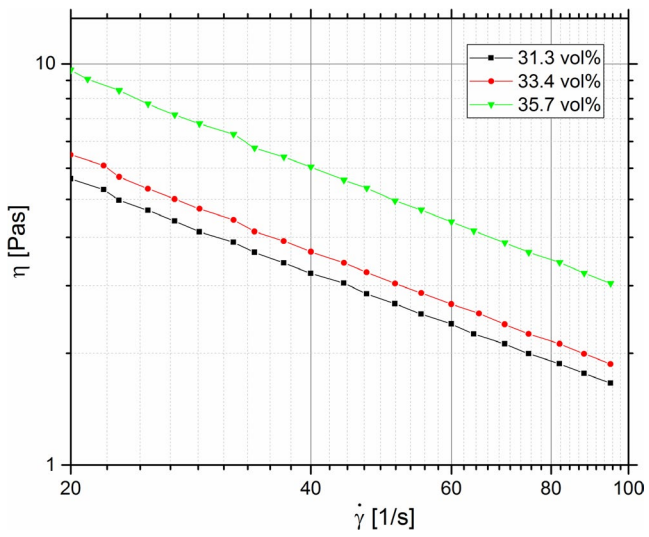

FIGURE 2 Dependence of viscosities of suspensions with various solid loadings with the shear rate

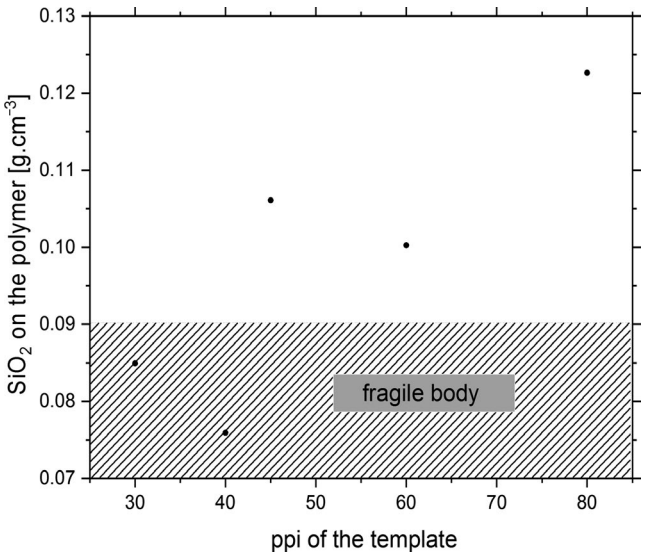

FIGURE 3 Map of feasibly of green bodies for different polymer templates

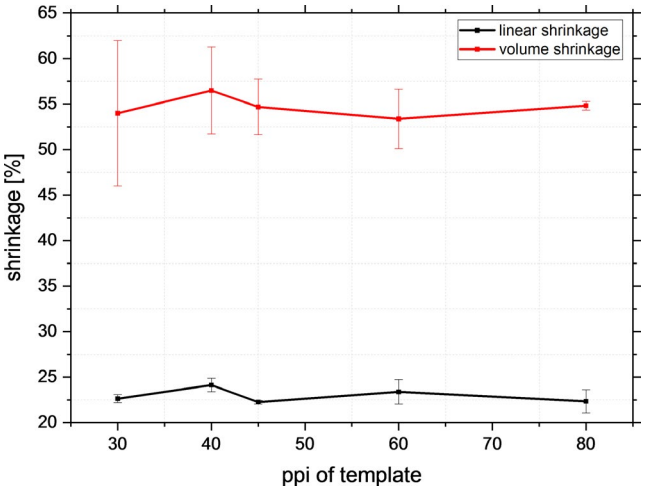

FIGURE 4 Linear (from edge to edge) and volume shrinkage of sintered sponges as a function of the pore size of the sponges

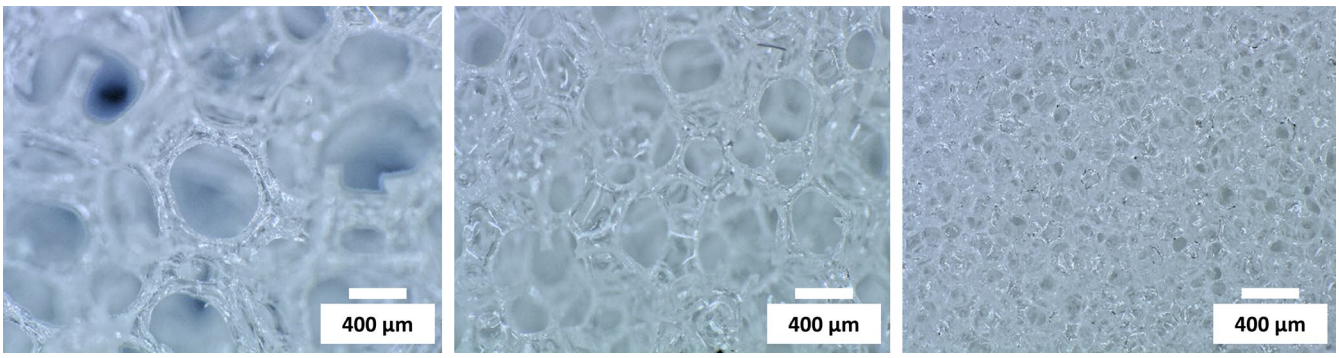

FIGURE 5 Light microscope pictures. Left: glassy sintered sponge out of a 30 ppi template; middle: sintered sponge out of a 45 ppi template; right: sintered sponge out of an 80 ppi template

of the shear rate. A shear thinning behavior is present and, with increasing solid loadings, the viscosity increases as well. At a shear rate of 50 s^{-1}, the 35.7 vol%. solid loading suspension reaches a viscosity of about 5 Pa, allowing a homogeneous coating of the struts of the polymer sponge.

Burning out the polymer is a very important step for obtaining manageable and stable green bodies. A special temperature regime must be applied, and a sufficient concentration of SiO_2 on the struts is necessary to avoid the framework collapse. Therefore, the solid loading of the suspension must be high. The dependence of the SiO_2 amount on a given volume of template on the solid loading was determined for templates of 30, 40, 45, 60, and 80 ppi. In general, for higher ppi values, the SiO_2 loading on the polymer is higher, and the green bodies become manageable after the burning out process. Otherwise, the sponges are too fragile to handle. In contrast, the number of closed pores increases because it is more difficult to wring out the excess suspension. If templates with a pore count of 45 ppi and larger are used, a higher SiO_2 loading is achieved. This fact could indicate a larger number of closed pores, but this hypothesis could not be confirmed.

Regardless of the suspension used, it appears that there is a threshold that must be reached for manageable green bodies. Below this value, of approximately 0.09 g cm^{-3} of template, it was not possible to get the desired structure through the burning out process, as shown in Figure 3.

3.2 | Sintering and crystallization behavior

After the burning out step, the obtained green bodies can be densified by viscous-flow sintering with the following sintering program:

$$\mathrm{RT} \xrightarrow{10^{\circ}\mathrm{C/min}} 1300^{\circ}\mathrm{C}\ \text{dwell time: } 12\ \text{min} \xrightarrow{20^{\circ}\mathrm{C/min}} \mathrm{RT}.$$

This leads to a mean linear shrinkage of about 23% and a mean volume shrinkage of 55% as observed in Figure 4 from the geometrical measurements. For both the green bodies and the sintered bodies, the geometry was determined using a caliper. As the ppi values become smaller, the cells become bigger and consequently the sponges structure gets more fragile. The error increases due to fragility and due to the uncertainty of the volume calculation out of three length measurements, which must be considered in the results.

After the thermal treatment, the initial green bodies can be transformed into transparent, open-celled foams. Transparency indicates that the amorphous character of the initial powder is still present. Accordingly, the sintered foams appear transparent as long as amorphous SiO_2 is present, as observed in Figure 5. Otherwise, the foam is white and opaque. Two reasons exist for the white color: either sintering was incomplete or the amorphous structure has changed into a crystalline one. In the latter case, the white color is probably caused by scattering of light at grain boundaries.

After sintering at two different temperatures, 1300 and 1350°C, the developed phases were analyzed employing XRD. The results are shown in Figure 6. When sintering is done at 1300°C, a typical pattern of amorphous SiO_2 can be

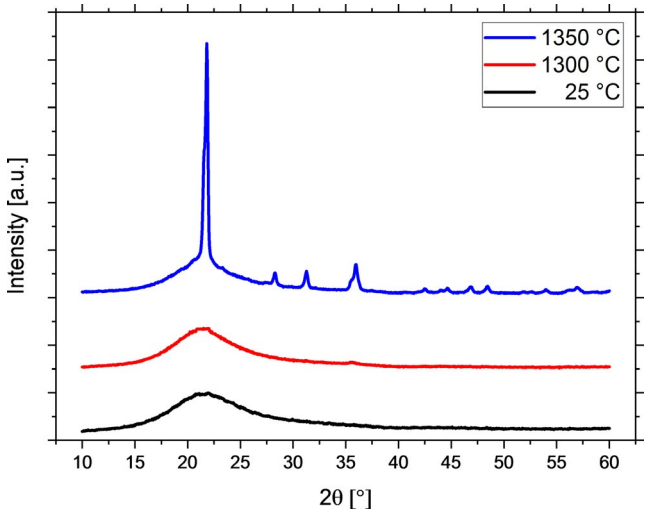

FIGURE 6 XRD patterns of sponges sintered at 1300 and 1350°C in comparison with the initial silica powder at room temperature

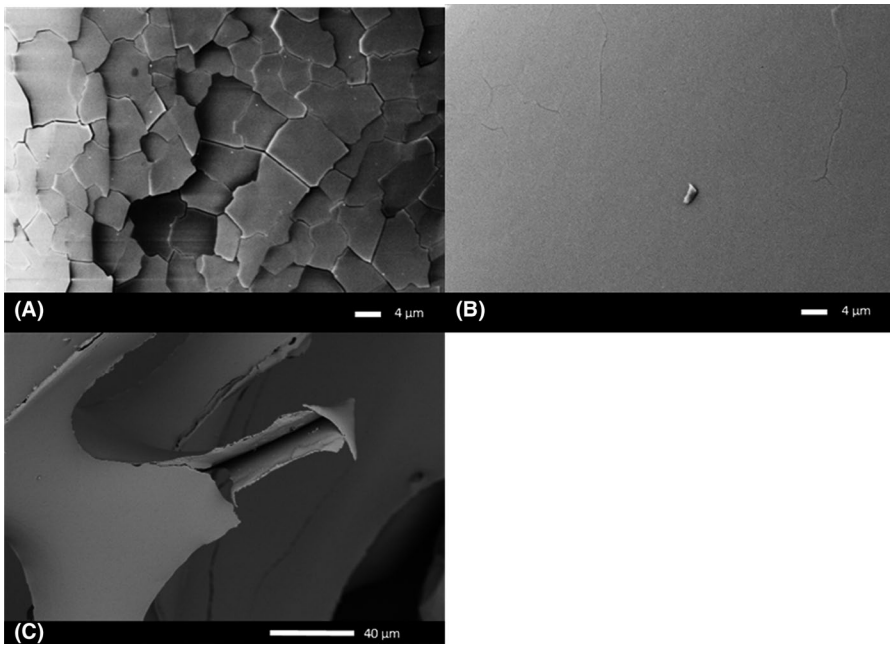

FIGURE 7 SEM images of A, a crystalline strut of a sintered sponge above 1350°C, B, an amorphous strut of a sintered sponge at 1300°C, C, a broken strut, where the triangle pore resulting from the burned-out polymer is shown

observed. The broad peak near $2\theta = 22°$ is attributed to the short-range order in amorphous silica, which is similar to the initial silica powder at 25°C. Above a temperature of 1350°C, SiO_2 foams starts to crystallize; the sharp peaks of the XRD pattern correspond to crystalline cristobalite as the only detectable phase.

By SEM analysis, surfaces of transparent and nontransparent foams were imaged. A micrograph of a nontransparent strut is depicted in Figure 7A). The surface is flaky, probably due to the crystallization process. This coarse surface contributes to the loss of transparency. In contrast, in Figure 7B), for a foam sintered at 1300°C, a smooth surface can be observed with only few defects. Consequently, the struts are not crystallized and appear transparent. In addition, in Figure 7C), an amorphous broken strut is shown, where the porosity in the struts resulting from the burning of polymer template is observed.

The sintered glassy sponges were investigated by µ-CT measurements. Therefore, a segmentation of the µ-CT images and follow-up calculations were performed by a Python algorithm based on scikit-image.24-26 First, a binary 3D stack was generated by Yen thresholding, that is, maximizing the entropic correlation between background and foreground voxel cells in the 3D grayscale stack.27 Small objects below a volume of 1000 voxel cells were regarded as artifacts due

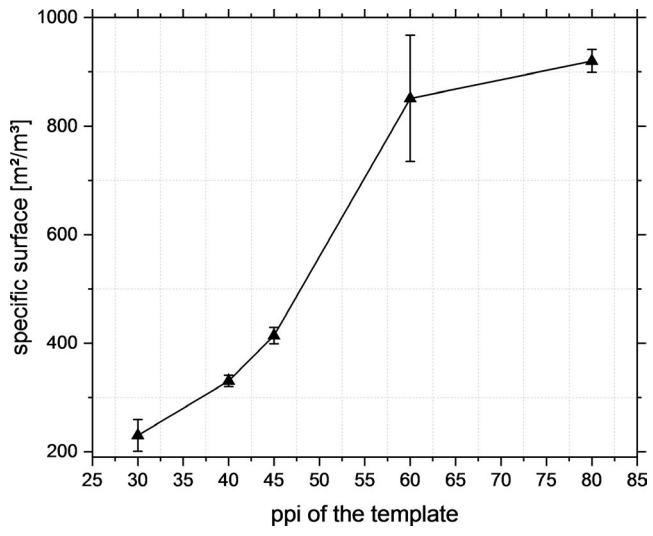

FIGURE 8 Specific surface of the sintered glass sponges as a function of the ppi value of the template

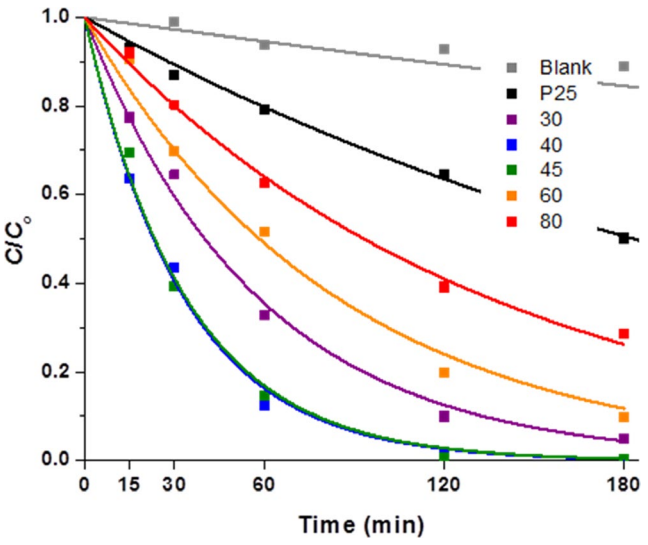

FIGURE 9 Evolution of the normalized Cr(VI) concentration (C/C_0) with the irradiation time for the photocatalytic reduction in the presence of EDTA. Experimental conditions: $[K_2Cr_2O_7] = 0.4$ mmol/L, [EDTA] = 1 mmol/L, pH 2, $E_{365nm} = 3500$ µW/cm^2, $T = 25$°C. The lines represent the adjustment of the curves to Equation (1)

TABLE 2 Characteristics of the sponges related to the fabrication process: percentage porosity of the sintered sponges, amount of TiO_2 attached by immersion in a P25 suspension, percentage of Cr(VI) transformation at 3 h of UV irradiation

Sample (ppi)	Porosity [%]	TiO_2 (P25) coating [mg]	Transformation of Cr(VI) in 3 h irradiation [%]
30	91.5	—[a]	94.5
40	92.3	—[a]	100
45	89.2	7.25	100
60	88.7	8.35	93.5
80	84.4	3.85	71
P25		2.1	50
blank		—	12

[a]The amount of attached TiO_2 could be not determined.

to measurement noise and thus removed from the 3D stack. A morphological closing was used to fill the voids left from preform burnout. The surface calculation was made to exclude closed porosity from the surface calculation, since the closed pores make only a surface contribution to the activity. The surface calculation was performed by a modified marching cubes algorithm to create a triangular mesh, whose surface was then calculated and divided by the total volume to obtain a specific area.28 The sponge volume for specific area calculations was obtained as the volume of the measurement convex hull. The calculated specific surfaces for sintered sponges as a function of the ppi value of the polymer templates are shown in Figure 8.

Up to 60 ppi, an exponential behavior is clearly seen relating the specific surface and the ppi value of the template but, at 80 ppi, the influence of the closed porosity deviates from this behavior. This may be a consequence of the manufacturing process of the polymeric templates and on their SSAs. The reason for the large error bars for samples with 60 ppi is probably that there is a transition where some isolated cells of the sponge are closed due to the small cell size. When some cells are closed, the values begin to scatter. This is especially the case for 60 ppi samples. In contrast, the error bars for 80 ppi becomes comparably smaller, because of the bigger number of cells, which improves the statistics.

3.3 | Photocatalytic activity of the SiO_2 sponges coated with TiO_2

The photocatalytic activity of the SiO_2 sponges coated with TiO_2 was tested with the Cr(VI)/EDTA system ($[Cr(VI)]_0$ = 0.8 mmol/L; [EDTA]/[Cr(VI)] = 1.25; pH 2; E_0 = 3520 mW cm^{-2}), according to previous papers of the group (eg, Refs. [14, 15, 16]). EDTA was used as a sacrificial synergetic agent to improve Cr(VI) transformation.

Figure 9 presents the results of normalized Cr(VI) concentration temporal profiles using the TiO_2-coated sponges and the coated glass slide containing 2.1 mg of TiO_2, together with the results obtained in the absence of photocatalyst under similar conditions (blank). It can be seen that the

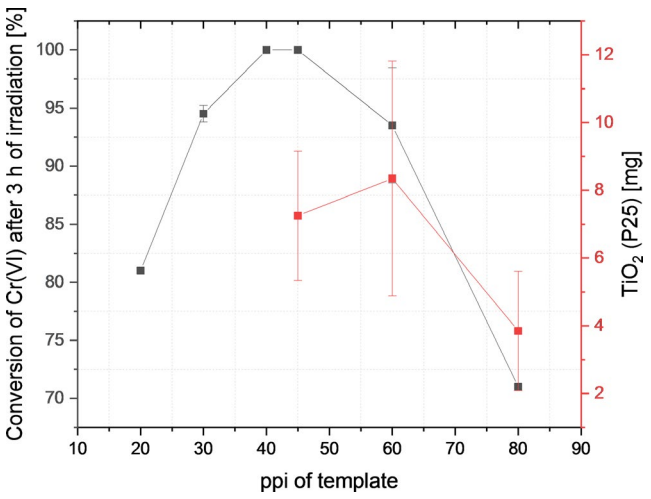

FIGURE 10 Conversion of Cr(VI) after 3 hours of irradiation and amount of TiO_2 as a function of the ppi of the template

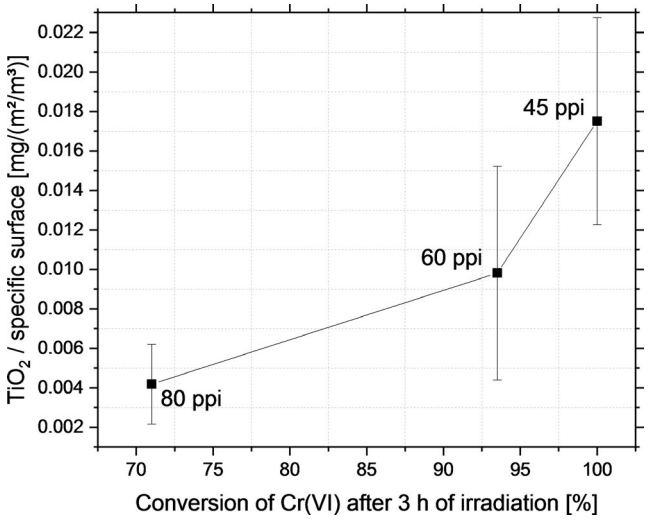

FIGURE 11 Conversion of Cr(IV) after 3 hours irradiation as a function of the amount of TiO_2 normalized by the specific surface of the sponges

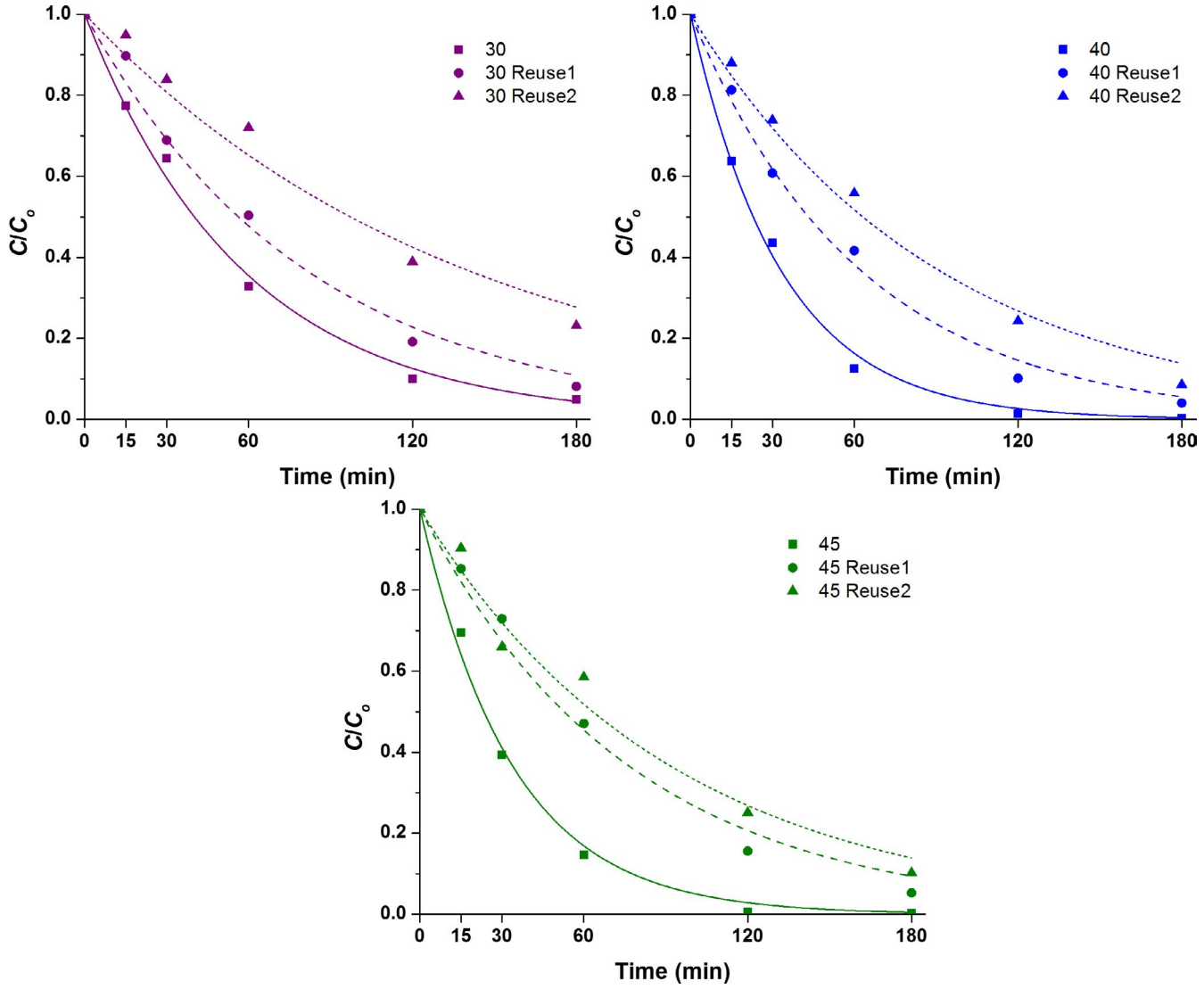

FIGURE 12 Evolution profile of the normalized Cr(VI) concentration (C/C_0) with the irradiation time for the photocatalytic reduction in the presence of EDTA. Experimental conditions: $[K_2Cr_2O_7] = 0.4$ mmol/L, [EDTA] = 1 mmol/L, pH 2, $E_{365nm} = 3500$ μW/cm^2, $T = 25$°C. First use: squares and continuous lines. Second use (Reuse 1): circles and discontinuous lines. Third use (Reuse 2): triangles and dotted lines. (A) 30 ppi; (B) 40 ppi; (C) 45 ppi

photocatalytic Cr(VI) reduction with all the coated samples is faster than the reduction in the absence of TiO_2, and that all coated sponges exhibit a higher photocatalytic activity than the P25 glass slide sample. The experimental points for both the homogeneous and the heterogeneous reactions could be adjusted with Equation (1):

$$C/C_0 = e^{-kt} \quad (1)$$

where C is the Cr(VI) concentration in solution, C_0 is the Cr(VI) concentration at the beginning of the photocatalytic test, and k is the pseudo-first order kinetic constant. The fitting curves using Equation (1) show a good agreement ($R^2 > 0.97$) with the experimental points. In contrast with other supported photocatalysts,19-21,29 a zero-order term to describe the reaction on the immobilized catalyst surface was not necessary in the present case. The pseudo-first order kinetic regime can be attributed to the higher surface areas of the photocatalyst that cannot be saturated by adsorbed chromium, making the reduction rate dependent on the Cr(VI) concentration in solution, as in the case of the homogeneous systems. Similar k values for Cr(VI) transformation were reported for long nanotubular TiO_2 coatings made by anodic oxidation.21

Table 2 shows some characteristics of the sponges related to the fabrication process: the porosity of the sintered sponges, the amount of TiO_2 attached by immersion in a P25 suspension, and the percentage of Cr(VI) transformation at 3 hours of UV irradiation.

It can be observed that the photocatalytic activity of the coated sponges for Cr(VI) transformation increased with the porosity of the sponges up to 40 and 45 ppi samples and then decrease for samples with higher ppi values. These

TABLE 3 Amount of TiO_2 attached to the sponges by immersion in P25 suspensions, performance of the TiO_2-coated sponges in successive photocatalytic tests of Cr(VI) transformation after 3 h of UV irradiation and corresponding kinetic constant, k [min^{-1}] extracted from Figure 12

	TiO_2 coating	1st Use		Reuse 1		Reuse 2	
Sample	P25 [mg]	% Cr(VI) transformation	k [$min^{-1} \times 10^{-2}$]	% Cr(VI) transformation	k [$min^{-1} \times 10^{-2}$]	% Cr(VI) transformation	K [$min^{-1} \times 10^{-2}$]
30	—[a]	95	1.73	92	1.23	77	0.71
40	—[a]	100	3.02	96	1.60	91	1.10
45	5.9	100	2.96	95	1.31	90	1.10
60	10.8	90	1.19	95[b]	2.10	84	0.81
80	5.1	71	0.74	94[b]	1.31	93[b]	1.12
P25	2.1	50	0.38	—	—	—	—
blank	—	12	<0.01	—	—	—	—

[a]The amount of attached TiO_2 could be not determined.

[b]P25 in suspension detached from the sample was observed at the end of the photocatalytic experiment.

photocatalytic results can be related to the accessibility of light and reagents in the samples: the accessibility would increase up to a certain ppi value, but then the accessibility would be hindered, as shown in Figure 10. An optimal photocatalytic activity can be found for the 45 ppi sample in relationship with the fabrication process of the sponges. It means that there is an optimum density and porosity of the sponges when coating the TiO_2 nanoparticles for photocatalytic applications. This is a very promising result because, for 45 ppi or high, the mechanical stability of the sponges is also very good. This combination of both the stability and the activity is encouraging for further photocatalytic applications. These results could be proved when the conversion of Cr(IV) was plotted over the amount of TiO_2 normalized by the specific surface of the sponges (Figure 11).

3.4 | Reuse of samples

The results of photocatalytic tests after three consecutive experiments reusing the 30, 40, and 45 ppi samples are shown in Figure 12. The percentage of Cr(VI) transformation and the kinetic constant corresponding to each experiment are shown in Table 3.

When the 30, 40, and 45 ppi sponges were reused, the photocatalytic activity decreased, attaining at least 70% Cr(VI) transformation on the third use. It is important to remember that no reactivation of the samples was performed between each test.

In the cases of the 60 and 80 ppi sponges, an excessive detachment of P25 during the reuses was observed, evidenced by the high Cr(VI) transformation due to the presence of P25 in suspension. This detachment can be related to the more closed structure of the 60 and 80 ppi sponges that makes the penetration and adherence of P25 difficult in comparison with the samples with more open structure (30, 40, and 45 ppi), in which the P25 detachment was not significant.

4 | CONCLUSIONS

In this work, the influence of probably the most important steps in the replica method for obtaining SiO_2 transparent foams, and its geometrically characterization using light microscopy and μ-CT for a variation of pore sizes have been discussed, together with the photocatalytic performance of TiO_2-coated sponges evaluated with the Cr(VI) reductive photocatalytic transformation in the presence of EDTA.

The following effects on the preparation of the SiO_2 transparent foams have been evaluated: (a) slurry preparation and its influence on the coating process, (b) burning out the polymeric template under the condition where stable green bodies are obtained, and (c) correlation between the sintering temperature and the optical properties. It has been found that the stability of the SiO_2 slurries plays a major role in the whole replication method.

Transparent silica sponges with high ppi were successfully obtained as well as its coverage with TiO_2 nanoparticles. Taking into account the photocatalytic transformation of Cr(VI) as a function of geometrical parameters, it is shown that an optimum between TiO_2 concentration and SSA for 45 ppi samples is observed. The photocatalytic activities increase two times in comparison with TiO_2-coated glass plates due to the high specific area. In addition, it was checked that the sponges after three times reuse test presented a good efficiency of about 70% of the transformation.

The application of the SiO_2 sponges as a substrate for TiO_2 immobilization for heterogeneous photocatalysts for water and air decontamination is promissory for application in photoreactors for transformation of pollutants.

ACKNOWLEDGMENTS

The authors thank the German Research Foundation (DFG) for funding the Research Group FOR 583 "Solid Sponges - Application of monolithic network structures in process engineering," CONICET, Agencia Nacional de Promoción Científica y Tecnológica (ANPCyT) from Argentina under PICT-2015-208 and PICT-2017-2133, and BioCriticalMetals – ERAMIN 2015 grant. SPUK – Strategic Partnership Universidad Nacional de San Martin, Argentina (UNSAM), Karlsruher Institute for Technologies, (KIT), Innovation und International.

ORCID

Fabian J. Altermann https://orcid.org/0000-0002-3580-8857
Ethel C. Bucharsky https://orcid.org/0000-0001-8236-119X
Karl G. Schell https://orcid.org/0000-0002-9418-7763

REFERENCES

1. Reichelt E, Heddrich MP, Jahn M, Michaelis A. Fiber based structured materials for catalytic applications. Appl Catalysis A: General. 2014;476:78–90.
2. Okada K, Kuboyama KI, Takei T, Kameshima Y, Yasumori A, Yoshimura M. In situ zeolite Na-X coating on glass fibers by soft solution process. Microporous Mesoporous Mater. 2000;37(1–2):99–105.
3. Deng Z, Balkus KJ. Pulsed laser deposition of zeolite NaX thin films on silica fibers. Microporous Mesoporous Mater. 2002;56(1):47–53.
4. Sero ET, Siziba N, Bunhu T. Biophotonics for improving algal photobioreactor performance: a review. Int J Energy Res. 2019;2020:1–22.
5. Hegedus G, Sarkadi T, Czigány T. Analysis of the light transmission ability of reinforcing glass fibers used in polymer composites. Materials. 2017;10(6):637.
6. Jacob A, Bucharsky EC, Schell KG. The application of transparent glass sponge for improvement of light distribution in photobioreactors. J Bioprocess Biotech. 2012;02(01). 1000113.
7. Colombo P. Ceramic foams: fabrication, properties and applications. Key Eng Mater. 2001;206-213:1913–8.
8. Sepulveda P. Gelcasting foams for porous ceramics. Am Ceram Soc Bull. 1997;76(10):61–5.
9. Thijs I, Luyten J, Mullens S. Producing ceramic foams with hollow spheres. J Am Ceram Soc. 2004;87(1):170–2.
10. Luyten J, Mullens S, Cooymans J, De Wilde AM, Thijs I, Kemps R. Different methods to synthesize ceramic foams. J Eur Ceram Soc. 2009;29(5):829–32.
11. Studart AR, Gonzenbach UT, Tervoort E, Gauckler LJ. Processing routes to macroporous ceramics: a review. J Am Ceram Soc. 2006;89(6):1771–89.
12. Schwartzwaelder K, Sommer A. Method of making a porous shape of sintered refractory ceramic articles. United States Patent No. 3090094, 1963.
13. Lange FF, Thousand MK, Thousand Oaks, CA (USA) KT Rockwell ISC. Open-cell, low-density ceramics fabricated from reticulated polymer substrates. 1987; Available from: https://www.osti.gov/servlets/purl/6073672.
14. Bucharsky EC, Schell KG, Oberacker R, Hoffmann MJ. Preparation of transparent glass sponges via replica method using high-purity silica. J Am Ceram Soc. 2010;93(1):111–4.
15. Löffler FB, Bucharsky EC, Schell KG, Hoffmann MJ. Preparation and characterization of transparent SiO_2 sponges for water treatment. Ceram Forum Int. 2018; cfi/BER. D. Available from: www.iam.kit.edu.
16. Fredrich JT, Menéndez B, Wong TF. Imaging the pore structure of geomaterials. Science. 1995;268(5208):276–9.
17. Robert D, Keller V, Keller N. Immobilization of a semiconductor photocatalyst on solid supports: methods, materials and applications. Photocatalysis and Water Purification. From Fundamentals to Recent Applications. 2013;145–78.
18. Diamanti MV, Ormellese M, Pedeferri MP. Application-wise nanostructuring of anodic films on titanium: a review. J Exp Nanosci. 2015;10(17):1285–308.
19. Traid HD, Vera ML, Ares AE, Litter MI. Advances on the synthesis of porous TiO_2 coatings by anodic spark oxidation. Photocatalytic reduction of Cr(VI). Mater Chem Phys. 2017;191:106–13.
20. Vera ML, Leyva G, Litter MI. Simple TiO_2 coatings by sol-gel techniques combined with commercial TiO_2 particles for use in heterogeneous photocatalysis. J Nanosci Nanotechnol. 2017;17(7):4946–54.
21. Vera ML, Traid HD, Henrikson ER, Ares AE, Litter MI. Heterogeneous photocatalytic Cr(VI) reduction with short and long nanotubular TiO_2 coatings prepared by anodic oxidation. Mater Res Bulletin. 2018;97:150–7.
22. Litter MI. Last advances on TiO_2 -photocatalytic removal of chromium, uranium and arsenic. Curr Opinion Green Sustainable Chem. 2017;6:150–8.
23. ASTM Annual Book of ASTM standards. Am Soc Test Mater. Berlin, Germany: Beuth Verlag GmbH; 1997;D1687–92.
24. Oliphant TE. Python for scientific computing python overview. Comput Sci Eng. 2007;10–20.
25. Millman KJ, Aivazis M. Python for scientists and engineers. Comput Sci Eng. 2011;13(2):9–12.
26. van der Walt S, Schönberger JL, Nunez-Iglesias J, Boulogne F, Warner JD, Yager N, et al. Scikit-image: image processing in python. PeerJ. 2014;2014(1):1–18.
27. Yen J-C, Chang F-J, Chang S. A new criterion for automatic multilevel thersholding. Notes. 1995;4(4):5436–9.
28. Lewiner T, Lopes H, Vieira AW, Tavares G. Efficient implementation of marching cubes' cases with topological guarantees. J Graph Tools. 2003;8(2):1–15.
29. Kleiman A, Márquez A, Vera ML, Meichtry JM, Litter MI. Photocatalytic activity of TiO_2 thin films deposited by cathodic arc. Appl Catalysis B: Environ. 2011;101(3-4):676–81.

How to cite this article: Löffler FB, Altermann FJ, Bucharsky EC, et al. Morphological characterization and photocatalytic efficiency measurements of pure silica transparent open-cell sponges coated with TiO_2. *Int J Appl Ceram Technol*. 2020;00:1–10. https://doi.org/10.1111/ijac.13504